Chapter 3

Ternary Nanocomposite of red P, reduced Graphene Oxide and Graphitic Carbon Nitride (red P-rGO-g-C_3N_4) as Metal Free Electro-catalysts for Hydrogen Evolution Reaction

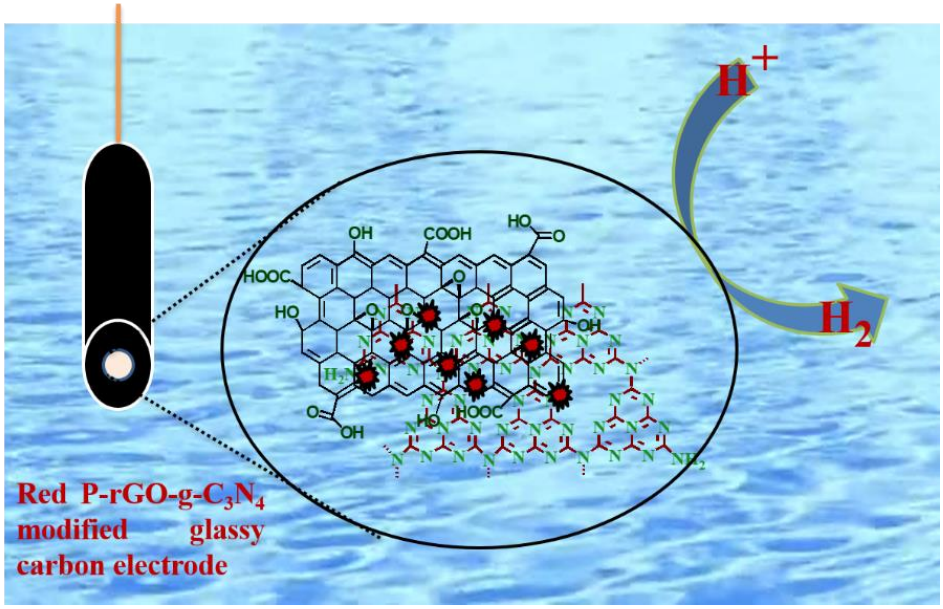

This chapter highlights the one-step hydrothermal synthesis of metal-free ternary nanocomposites red P-rGO-g-C_3N_4 and its successful implication as HER electrocatalysts to explore the alternatives of noble metal platinum (Pt) based HER catalyst.

3.1 Introduction

The present world is exploring multiple options for clean, cheap and renewable sources of energy to take on the energy crisis and hydrogen as an energy carrier generated from electrochemical water splitting phenomenon driven by renewable electricity serves as one of the best options. Hydrogen molecule has highest energy density per unit mass and on combustion produces only water as a by-product. Hydrogen as a fuel is deployed into Fuel cell electric vehicles (FCEVs) and ready to take on fossil fuels-based energy. [110,111] Platinum has proved to be the most efficient electrocatalyst for H_2 generation by water splitting to date, but it owes certain limitations to be used at commercial scale such as higher cost and low availability. [112] This has led researchers to explore non-noble metal and metal-free based electrocatalysts. It includes non-noble metal electrocatalysts like transition metal dichalcogenides/nitrides/carbides and heteroatom doped transition metal phosphides and sulphides. [113-121] Use of nanostructured catalysts made up of earth-abundant elements such as carbon, nitrogen and phosphorous is another wise choice for HER electrocatalyst.[60] Hence, the quest over environment benign metal-free electrocatalyst is going on. [122-124]

g-C_3N_4 is a polymeric two-dimensional nitrogen-rich semiconductor with high thermal and chemical stability. Lots of research have been done over its visible light-driven photocatalytic performance owing to its band gap of 2.7eV in the visible spectrum. [31,33,89,125,126] However, only a few reports are available on the electrochemical performance of this material. g-C_3N_4 alone exhibits good resistivity towards HER (Hydrogen evolution reaction) in acidic media and ORR (Oxygen reduction reaction) in basic media due to its low electrical conductivity, fewer defective sites and low surface area. [122] However, it can be brought into

the wide electrochemical application by making the polymeric g-C_3N_4 porous and addition of an optimum amount of conducting species. Reduced graphene oxide (rGO) is two-dimensional carbon material with excellent electrical and thermal conductivity with high surface area. An optimum weight fraction of rGO is expected to be a better choice to enhance the electron transition properties of 2D g-C_3N_4. [127-130] Phosphorous has many properties similar to nitrogen of g-C_3N_4 as both elements belong to the pnictogen family of the periodic table. Phosphorous has typically three kinds of allotropes red, white and black, among them red P is expected to be a cheaper, chemically stable, earth-abundant and has lower toxicity than other counterparts which makes it the best additive. Red P also has a high theoretical capacity of 2596 mA h^{-1} g to be used as anode material in sodium-ion batteries. [131] A number of metal phosphides have been reported to show robust HER performance and in most of them, phosphorous was taken as phosphate, phosphite or hypophosphite. [132-138] These phosphorous act as active sites like nitrogen of g-C_3N_4. Although the use of elemental red P in the electrocatalytic application is still limited owing to its less conductivity, however hydrothermal treatment for a longer time leads to size degradation and surface oxidation enhancing its conductivity and making it suitable to be used as an additive to enhance the electrocatalytic performance of 2D g-C_3N_4. Such modification of red phosphorous will provide more insight into the further use of elemental phosphorous to enhance the electrocatalytic HER activity.

In view of the above facts, we have successfully prepared different weight % of red P embedded rGO-g-C_3N_4 composite hydrothermally. At first, g-C_3N_4 was immobilized initially over optimum 5 weight % of GO by sonication method and then various red P-rGO-g-C_3N_4 composites were prepared by mixing different

amounts of elemental red P with GO-g-C_3N_4 at elevated temperature by hydrothermal treatment. In prolonged hydrothermal treatment at 200°C, GO gets reduced to rGO enhancing the conductivity of the entire composite, which was confirmed by heating GO alone hydrothermally under similar conditions. Graphitic and pyridinic nitrogen of g-C_3N_4 is considered as active sites for harbouring H^+ for further electrocatalytic reduction. Since, as-synthesized bulk g-C_3N_4 possess small specific surface area and small pore volume, which are not conducive for electron and electrolyte transfer during electrochemical activity. However, Prolonged Hydrothermal treatment enhances the porosity of entire composites and creates more defective sites; hence more active sites for H^+ adsorption and faster electron transfer leading to increased HER performance. In the hydrothermal process at 200°C, red P degrades in size owing to high pressure and temperature, ultimately becoming an intimate part of the binary composite rGO-g-C_3N_4. In our experiment, we observed that increasing the weight % of P into rGO-g-C_3N_4 composites leads to enhancement in HER activity due to the generation of more active sites to catch H^+, however only an optimum amount of red P present in the ternary composite leads to the best HER activity among all, thereafter increasing the red P amount restricts the availability of active sites and fall in HER activity is observed. Therefore, red P concentration plays an important role to get the best HER performance from ternary P-rGO-g-C_3N_4 composites. A complete structural and morphological characterization of as-synthesized composites have been done including elemental analysis by XPS technique and surface area determination to observe the post-hydrothermal effect in the composites in later sections. This is the composition tuning and post-hydrothermal synergistic effect of all the three

ingredients that results in increment in HER performance of metal-free triad as discussed in detail in result and discussion section.

3.2 Experimental Sections

3.2.1 Materials

Melamine (Extra Pure) and Red phosphorous were purchased from Loba Chemie, India and Spectrochem Pvt Ltd, India respectively. Graphite powder (< 20μm) was ordered from Sigma Aldrich, India. Ethylene glycol was purchased from Merck, India. All these chemicals were used without further purification. Ultrapure Millipore water (18.3 MΩ) was used for the preparation of all electrochemical solutions.

3.2.2 Synthesis of g-C_3N_4

The bulk g-C_3N_4 was prepared by heating 5.0 g of melamine powder into the alumina crucible covered with lid in the muffle furnace at 550°C (ramping rate= 3.0 ° min^{-1}) and kept as such at 550°C for 4 hours. Thereafter, a crucible containing light yellow solid mass is allowed to cool at room temperature. The bulk g-C_3N_4 obtained was grounded into a fine powder using agate-mortar and preserved for further characterizations.

3.2.3 Synthesis of Graphene Oxide (GO)

Graphene Oxide (GO) was synthesized by improved Hummer's method. Firstly, 1.0g of graphite powder was treated by 6.0g of $KMnO_4$ in a large beaker (capacity=2000.0L) in presence of a mixture of concentrated acids having 120.0 ml conc. H_2SO_4 and 12.2 ml H_3PO_4 in the ratio of 9:1. The reaction mixture was stirred at 50°C and kept for 12h to ensure complete exfoliation of the graphitic sheet. After that, the reaction mixture is cooled to room temperature and ice water of almost

equal volume was poured into the reaction mixture followed by 3.0 ml of 30% H_2O_2. Finally, the whole solution was centrifuged at 4000 rpm for 4h and the supernatant was discarded by decantation. The obtained brownish solid (GO) was washed with 200 ml of distilled water, followed by 200 ml of 30% HCl solution several times to reach the neutral pH of 7. It was again washed with 200ml of ethanol two times. Thus, as-synthesized GO was dried at 60°C in a vacuum oven for 12 h.

3.2.4 Synthesis of Red P-rGO-g-C_3N_4 Composite

Prior to the synthesis of red P-rGO-g-C_3N_4 composite, g-C_3N_4 was immobilized over aqueous dispersion of GO by sonication method. Typically, aqueous dispersion of 100 mg g-C_3N_4 was added drop-wise into another aqueous dispersion of GO (5 wt. %) sonicated for 2 hours and then the resultant mixture was again sonicated for another 1 hour. The binary GO-g-C_3N_4 mixture was filtered and dried in a vacuum oven for 12 hours at 60°C. Thereafter, in order to synthesize 10% red P-rGO-g-C_3N_4, 30 mg GO-g-C_3N_4 was stirred into ethylene glycol for 1 hour and then 3.0 mg red P suspension in water was added into it. The solution mixture was stirred for another 1hour and transferred into a 25.0 mL Teflon lined stainless steel autoclave (filled to 80% of its capacity). The autoclave was kept in the oven at 200°C for 16 hrs. Finally, the reaction mixture was centrifuged to remove the supernatant and the composite precipitate was collected, dried in a vacuum oven at 60°C. This as-synthesized composite is designated as 10P-rGO-g-C_3N_4 throughout the manuscript. A schematic diagram representing the synthesis procedure is shown in Figure 3.1.

A similar method has been used to synthesize 20%, 30% and 40% red P-rGO-g-C_3N_4 composites and designated as 20P-rGO-g-C_3N_4, 30P-rGO-g-C_3N_4 and 40P-rGO-g-C_3N_4 respectively throughout the manuscript.

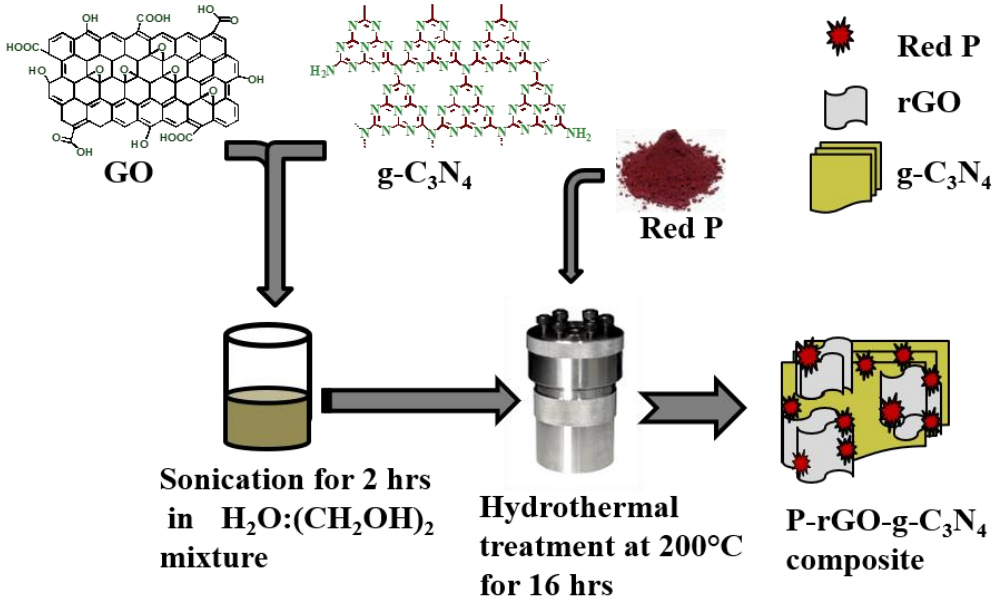

Fig. 3.1 Schematic diagram representing the synthesis of metal-free ternary nano-composite P-rGO-g-C_3N_4.

3.2.5 Preparation of Composite Ink and Electrode Modification

The composite ink was prepared as follows: First of all, 2.0 mg of the desired composite is dispersed into the 500 µL water-ethanol mixture (H_2O:C_2H_5OH::1:1). After that, 15 µl of Nafion solution (5wt%) is added into the resulting dispersion and sonicated for 2 h in order to make it homogenous. Prior to any electrochemical measurements, the GC electrode is polished first with 0.4 µm alumina powder over a polishing pad and 5.0 µL of as-prepared ink is loaded over the GC electrode (loading amount=0.271 mg cm^{-2}) then dried under IR lamp.

3.2.6 Instrumentations

Vibration spectrum (FT-IR) was obtained from a Thermo Scientific NICOLET iS5 instrument. XRD pattern was obtained from Rigaku miniflex 600 X-ray diffractometer, with Ni-filtered Cu $K\alpha_1$radiation (λ=1.54056Å) at a scan rate of $3°min^{-1}$. Field emission scanning electron microscope (FESEM) images were recorded from FEI NOVA NANO SEM 450 instrument. Transmission electron microscope (TEM) images were obtained from FEI, TECHNAI G^2 20 TWIN instrument at accelerating voltage of 200 kV. Both for FESEM and TEM, the sample preparation was carried out by casting the similar amount of dispersed materials in THF solvent. X-ray photoelectron spectra (XPS) were recorded on Thermo Fischer Scientific ESCALAB Xi+. N_2 adsorption-desorption isotherm was performed on the Quantachrome Autosorb instrument at 77K to get the specific surface area and pore size distribution of synthesized composites. Cyclic voltammetry (CV) and linear sweep voltammetry (LSV) were performed on CHI7044 model with three electrodes set up in which Ag/AgCl (in 3M KCl) is taken as reference electrode, Pt is taken as counter electrode and glassy carbon (diameter=3.0 mm) is taken as working electrode in 0.5M H_2SO_4 electrolyte. LSV was performed at a scan rate of 5 mV sec^{-1} in the potential window of +0.05 to -0.8 V (vs Ag/AgCl). CV was conducted using the same electrode set up in the potential window of 0.3 to 0.5 (*vs* RHE) owing to negligible faradic current in this region at scan rates of 20, 40, 60, 80, 100, 120, 140, 160, 180 and 200 mV sec^{-1}. All potential values were converted with reference to Reversible Hydrogen Electrode (RHE) using the equation

$$E_{RHE} = E_{Ag/AgCl} + 0.059\,pH + E^0_{Ag/AgCl} \quad \text{.....(Eq. 3.1)}$$

To test the current stability performance of the synthesized catalyst, 1.0mg catalyst is loaded over Toray carbon paper (area=1.0 cm^2) and taken as working electrode while another same paper having an area of 3×1 cm^2 is used as the counter electrode. Time dependant, current density graph (Chronoamperometry graph) was plotted using AUTOLAB PGSTAT302 Model at static over the potential value of -670mV (vs.Ag/AgCl) for 2 h (7200 seconds) in 0.5M H_2SO_4 supporting electrolyte.

3.3 Results and Discussion

3.3.1 Structural Characterization of Prepared Ternary Nanocomposites

Figure 3.2 (a) shows the XRD patterns of g-C_3N_4, rGO-g-C_3N_4, Red P, 10P-rGO-g-C_3N_4, 20P-rGO-g-C_3N_4, 30P-rGO-g-C_3N_4 and 40P-rGO-g-C_3N_4. The g-C_3N_4 (JCPDS No. 87-1526) exhibits a strong diffraction peak at ~27.4° corresponds to the (002) crystallographic plane and is due to the stacking of g-C_3N_4 2D layers at an inter-layer distance of 0.326 nm. [33] Another minor diffraction peak appears at ~13.0° that corresponds to (100) plane characteristic of interplanar separation. The diffraction peak at ~27.4° is clearly visible in all composites having g-C_3N_4 as a base material. It means that g-C_3N_4 is not destroying its identity under the given synthesis environment. Similarly, rGO reduced hydrothermally (also *see* Appendix A Fig. A.1) exhibits its characteristics peak at ~24.8° corresponding to (002) plane but this peak disappears in all rGO containing composites due to very less amount (5 % w/w) of it in the composites. Diffraction patterns of commercial red P (JCPDS No. 44-0906) alone show its characteristics major peak at ~15.4° corresponding to (002) plane along with a hump ~34°. In all the red P containing composites, the intensity of peak ~15.4° increases with increasing weight % of red P and can be seen to appear as a small hump in 40P-rGO-g-C_3N_4. [139,140] We have also

determined the crystallite size of all the composites using the Debye-Scherrer equation (Eq. 3.2) as follow to check the addition of red P in different amount has affected the crystallite growth or not.

$$Particle\ (crystalline\ size) = \frac{0.94\ \lambda}{FWHM\ cos\theta} \text{.....(Eq. 3.2)}$$

Where, λ is the wavelength of the X-ray radiation (Cu Kα = 0.15406 nm), FWHM stands for full width at half maxima and θ is diffraction angle. The crystallite size of all the composites is in the range of 6.5 to 7.5 nm and this size is smaller to the grain size determined in SEM images due to the agglomeration of crystallites. It confirms the presence of red P in rGO-g-C_3N_4 composites does not affect the crystallite size.

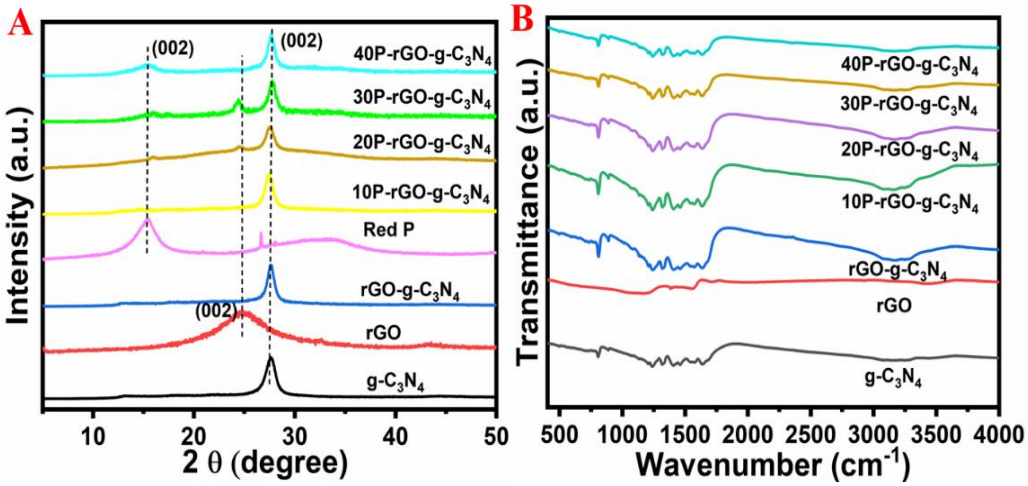

Fig. 3.2 (a). XRD patterns of g-C_3N_4, rGO, rGO-g-C_3N_4, Red P, 10-20-30-40P-rGO-g-C_3N_4 respectively (b) FT-IR spectrum of g-C_3N_4, rGO, rGO-g-C_3N_4, 10-20-30-40P-rGO-g-C_3N_4 respectively.

The identity of all components is further investigated by FTIR as shown in Figure 3.2 (b). The vibration peak at ~ 808 cm^{-1} is characteristic of the triazine unit of g-C_3N_4 which is visible in all composites. The vibration peaks in the fingerprint region from 1240 to 1635 cm^{-1} correspond to various stretching modes of aromatic C-N heterocycle and the vibration peak at ~3187cm^{-1} is the stretching mode of N-H of g-C_3N_4. [123,124] In the case of rGO, peak ~3440 cm^{-1} belongs to the stretching mode of ―OH and the vibration peak at ~1550 cm^{-1} confirms the presence of the sp^2 carbon network of graphene. [143] The disappearance of the C=O peak at 1734 cm^{-1} (characteristics of GO) verifies the conversion of GO into rGO during hydrothermal treatment. Although, because of very less amount (5%wt.) of rGO present in the g-C_3N_4 composites, these characteristics vibrations peaks are not much visible and may get merged with the peaks of g-C_3N_4. [127-130] Apart from these vibration peaks, all composites consist of vibration peaks related to red P and surface oxygen. The peak around 1634 cm^{-1} corresponds to P=O stretching mode, the P–O and P–P–O stretching modes have been merged around 1000 cm^{-1} to 1200 cm^{-1}. These all peaks are because of surfacial oxidation of red P during the synthesis process. [139] The FT-IR analysis of all red P-rGO-g-C_3N_4 composites show that introduction of red P into the composite and thermal treatment at 200°C for a prolonged time do not alter the original C-N backbone of g-C_3N_4 as no such vibrational peak showing any chemical bond formation between red P and g-C_3N_4 appears in the vibrational spectra. All the major vibration peaks of individuals and composites are tabulated in Appendix A Table A.1 for a proper correlation between individual components and composites.

Hence, both XRD and FT-IR analysis validates the structural identity of the as-prepared composites.

3.3.2 Morphological Analysis

To investigate the surface morphology, FE-SEM images of g-C_3N_4, rGO, red P, rGO-g-C_3N_4, 10P-rGO-g-C_3N_4, 20P-rGO-g-C_3N_4, 30P-rGO-g-C_3N_4 and 40P-rGO-g-C_3N_4 have been recorded on the same magnifications (200 KX) and shown in Figure 3.3. g-C_3N_4 exists in the form of compact and random flakes-type, while red P appears as fused flakes with relatively smaller size (100 to 300nm) with respect to that of g-C_3N_4 (*cf.* Fig. 3.3 (a) and Fig. 3.3 (c)). rGO prepared hydrothermally (Fig. 3.3 (b)) retains its sheet identity although hydrothermal treatment has caused rupturing of sheets as visible in FESEM images. In binary rGO-g-C_3N_4 (Fig. 3.3 (d)), rGO is seen spreading over the ruptured sheet of g-C_3N_4 and intermixes with g-C_3N_4 flakes. In the prepared P-rGO-g-C_3N_4 composites (Fig. 3.3 (e) to Fig. 3.3 (h)), red P is seen anchored over binary rGO-g-C_3N_4 heterostructures and can be easily identified as smaller fused identity. The effect of the hydrothermal treatment can be observed in Figure 3.3 (e) to 3.3 (h) as g-C_3N_4 appears more porous and red P gets more intimated in binary rGO-g-C_3N_4. The presence of red P over rGO-g-C_3N_4 surface increases with an increase in the concentrations of red P (*cf.* Fig. 3.3 (e), Fig. 3.3 (f), Fig. 3.3 (g) and Fig. 3.3 (h)) as also revealed in EDAX elemental mapping as shown in Fig. 3.4. Table 3.1 tabulated from EDAX data of FESEM shows the increasing concentration of phosphorous both as atomic % and weight % present in the composites, elemental mapping also confirms the increasing amount of red phosphorous in the P-rGO-g-C_3N_4 composites (also *see* Appendix A Fig. A.2). While comparing the FESEM images of P-rGO-g-C_3N_4 composites with that of g-C_3N_4 alone, it is visible that hydrothermal treatment has caused rupturing of sheets of binary rGO-g-C_3N_4 and intermixing of red P into the sheets. This leads to enhancement in surface area and generation of active sites for catalytic activity.

Hence, FESEM images show that the extent of porosity in red P impregnated rGO-g-C_3N_4 has higher owing to hydrothermal treatment and it has been further validated by surface area measurement in later sections.

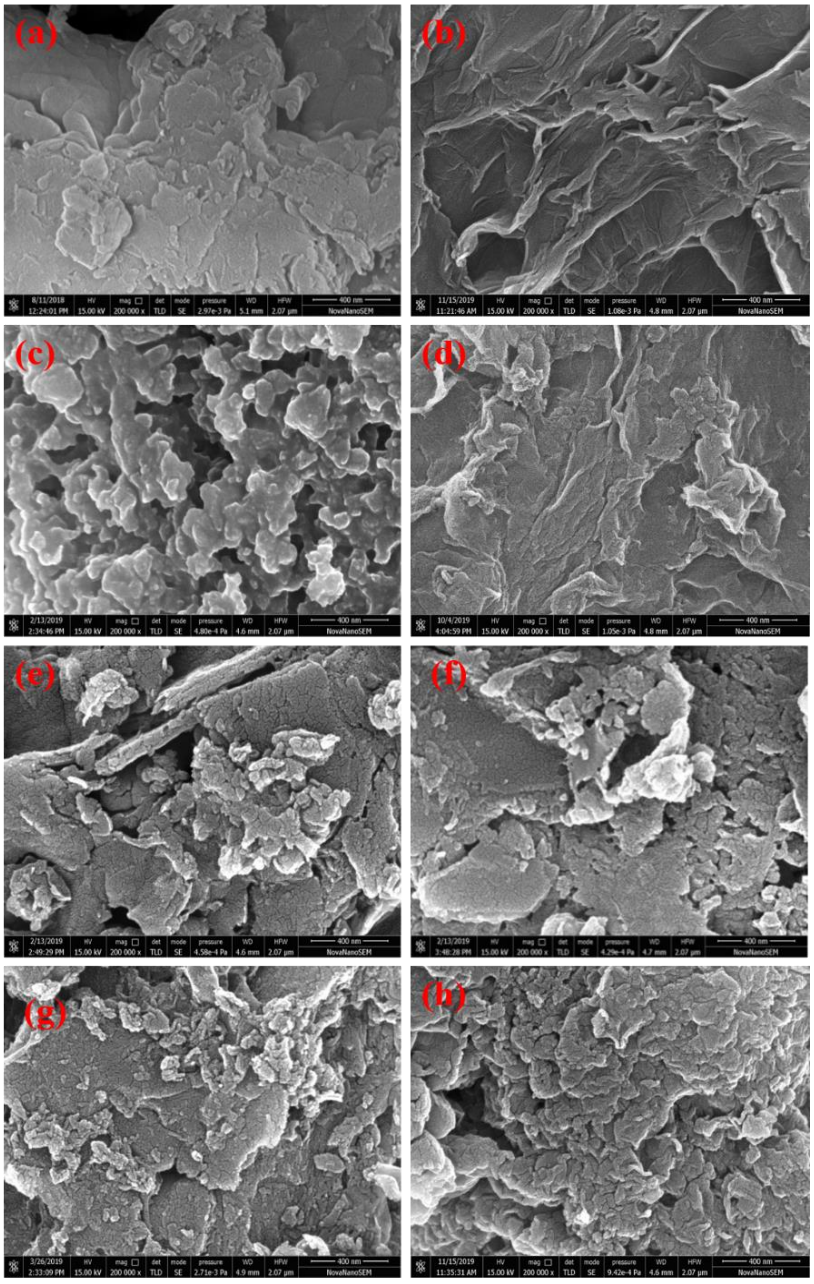

Fig. 3.3 FESEM images of (a) g-C_3N_4, (b) rGO, (c) Red P, (d) rGO-g-C_3N_4, (e) 10P-rGO-g-C_3N_4, (f) 20P-rGO-g-C_3N_4, (g) 30P-rGO-g-C_3N_4 and (h) 40P-rGO-g-C_3N_4.

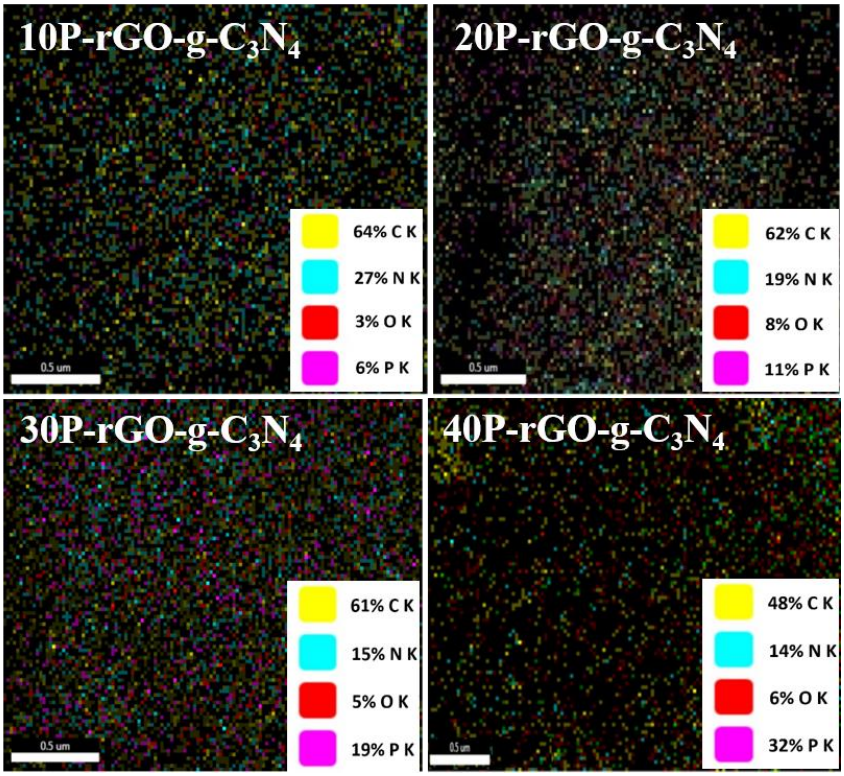

Fig. 3.4 EDX Elemental mapping of 10P-rGO-g-C_3N_4, 20P-rGO-g-C_3N_4, 30P-rGO-g-C_3N_4 and 40P-rGO-g-C_3N_4 composites.

Table 3.1 EDX data for % atomic phosphorous present in different P-rGO-g-C_3N_4 composites.

Sample	Weight % P	Atomic % P
10P-rGO-g-C_3N_4	1.06	0.46
20P-rGO-g-C_3N_4	2.33	1.01
30P-rGO-g-C_3N_4	3.99	1.74
40P-rGO-g-C_3N_4	7.69	3.41

Effect of hydrothermal treatment was further exemplified under transmission mode by TEM and HRTEM images of g-C_3N_4, rGO-g-C_3N_4 and 30P-rGO-g-C_3N_4 (Fig. 3.5). g-C_3N_4 alone can be seen as an intact sheet structure with no defects, while rGO-g-C_3N_4 and 30P-rGO-g-C_3N_4 appear as mangled structures compared to g-C_3N_4 which can be contributed to hydrothermal treatment.

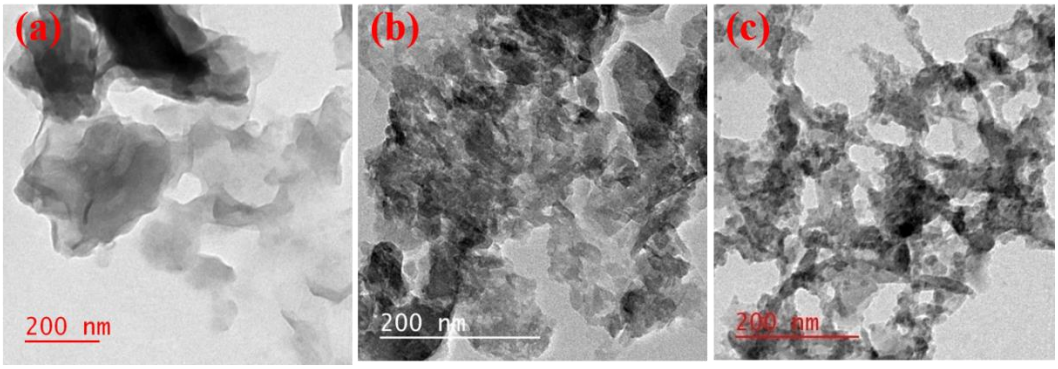

Fig. 3.5 TEM images of (a) g-C_3N_4, (b) rGO-g-C_3N_4 and (c) 30P-rGO-g-C_3N_4 respectively.

3.3.3 Elemental Analysis

To further verify the element present and has retained its identity in the composites, XPS was performed of g-C_3N_4, rGO-g-C_3N_4, 10P-rGO-g-C_3N_4, 20P-rGO-g-C_3N_4 and 30P-rGO-g-C_3N_4. The survey spectrum gives peaks of all individual elements as expected in the composites (*see* Appendix Fig. A.3). In Figure 3.6, high-resolution XPS peaks of C1s, N1s, O1s and P 2p of 10, 20 and 30 % P added ternary nanocomposites have been shown with each peak deconvoluted into assumed bonding state of elements. The high-resolution C_{1s} spectrum was deconvoluted and observed as an association of four characteristic peaks (Fig. 3.6 A to 3.6 C). The peak at ~288.30 eV is assigned to C-N coordination while the peak at ~ 288.50 eV is assigned to C-O. Similarly, the peak centred at ~284.70eV is designated to C-C

coordination and the peak at ~ 285.60 eV to C=C coordination. The high-resolution N_{1s} spectrum (Fig. 3.6 D to 3.6 F) consists of three deconvoluted peaks at ~399.40eV, 399.19eV and 401.21eV corresponding to graphitic N, pyridinic N and $–NH_2$/ =NH respectively. At the same time, a satellite peak around 405.20eV is supposed to appear because of positive charge delocalization. Similarly, the O_{1s} spectrum (Fig. 3.6 G to 3.6 I) exhibit two peaks centred at ~532.16eV and 534.00eV which are attributed to various surface O species. [141,142]

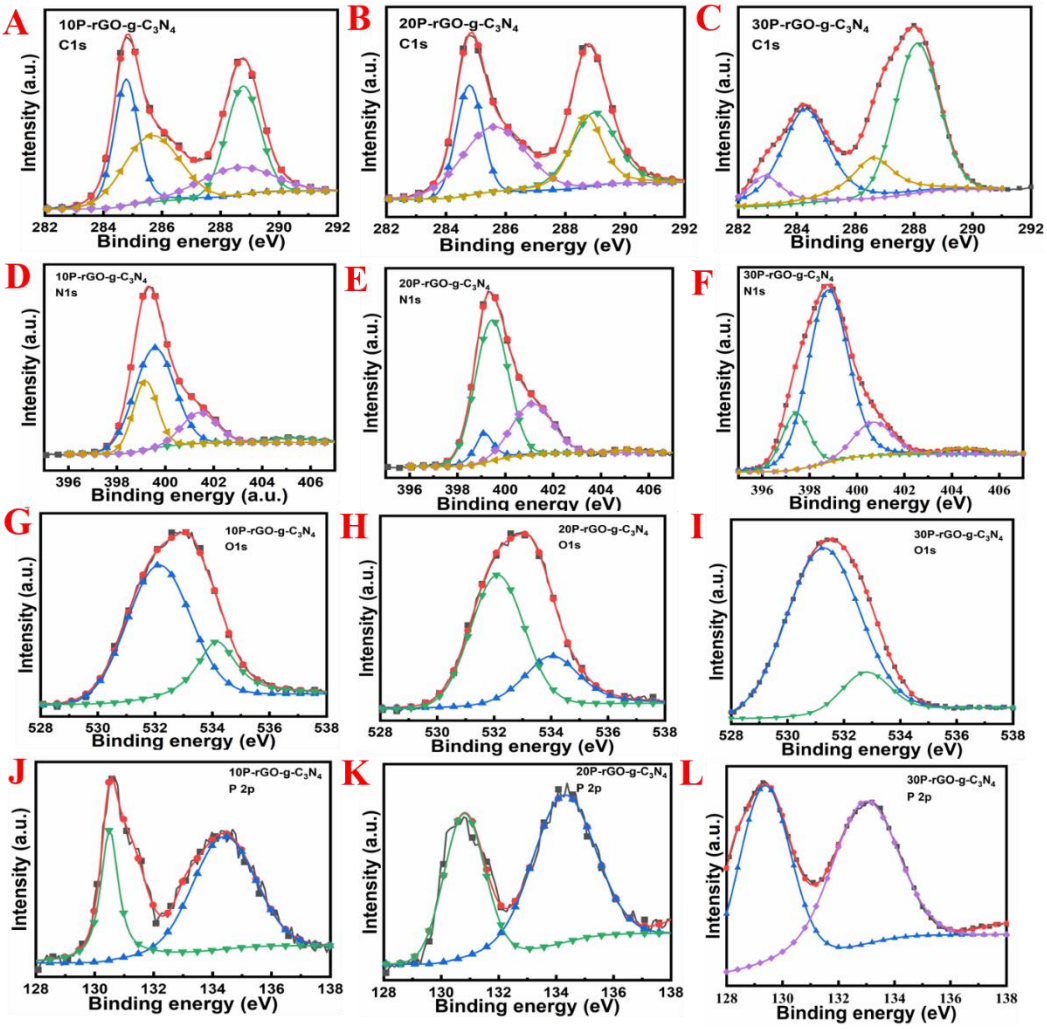

Fig. 3.6 Deconvoluted XPS peaks of C1s (A to C), N1s (D to F), O1s (G to I) and P2p (J to L) in 10P-rGO-g-C_3N_4, 20P-rGO-g-C_3N_4, and 30P-rGO-g-C_3N_4 respectively.

The high resolution P_{2p} spectrum (Fig. 3.6 J to 3.6 L) of 10P-rGO-g-C_3N_4, 20P-rGO-g-C_3N_4 and 30P-rGO-g-C_3N_4 again deconvoluted into two peaks at ~130.46eV and 134.20eV corresponding to P (0) and P (5+) state. The +5-oxidation state of P here is expected due to its oxidation during the synthesis process. [139,140,144] On the basis of these characterizations, we conclude that all individuals have retained their identity even in the composite state.

3.3.4 Surface Area Analysis

To get more insight into the surface features of the catalyst, we have measured surface area using N_2 adsorption-desorption isotherm at 77K (*see* Fig. 3.7 A). All three g-C_3N_4, rGO-g-C_3N_4 and 30P-rGO-g-C_3N_4 exhibit type IV isotherm behaviour with hysteresis loop of type H3. At relative pressure (P/P_0) <0.4, adsorption and desorption isotherm follow each other as a reversible process, while for relative pressure (P/P_0) range 0.4 to 1.0 has loop with no saturation implying mesoporous nature of both rGO-g-C_3N_4 and 30P-rGO-g-C_3N_4. BET plot gives the specific surface area of 12.776 m²/g, 85.904 m²/g and 62.236 m²/g for g-C_3N_4, rGO-g-C_3N_4 and 30P-rGO-g-C_3N_4 respectively. It signifies the effect of hydrothermal treatment as the surface area of 30P-rGO-g-C_3N_4 enhances by 5-fold in comparison to g-C_3N_4. Pore size distribution (*see* Fig. 3.7 B) determined from Brunauer-Joyner-Halenda (BJH) theory is located in ranges of 15 nm to up to 50 nm, while major pore-size distribution peak is spotted at 20 nm for rGO-g-C_3N_4 and 30P-rGO-g-C_3N_4, thereby confirming the mesoporous features of the composites. The pore volume of rGO-g-C_3N_4 is 0.138 cm^3g^{-1} which reduces to 0.115 $cm^3 g^{-1}$ in 30P-rGO-g-C_3N_4 owing to the incorporation of red P particles into the composite. Herein, we conclude that hydrothermal treatment has led to an increase in the porosity of the

composites and this porosity provides more interaction with ions and faster electron movement for catalytic activity.

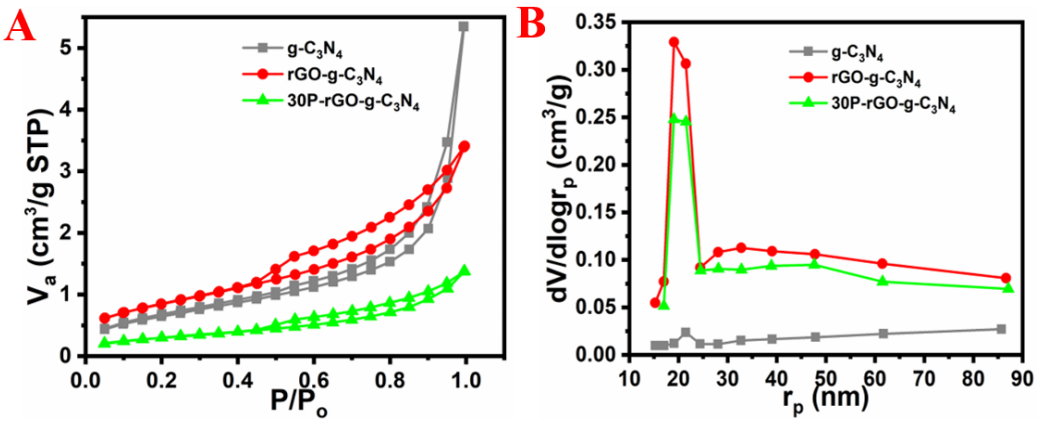

Fig. 3.7 (A) Nitrogen adsorption-desorption isotherm and (B) corresponding pore volume distribution curves of g-C_3N_4, rGO-g-C_3N_4 and 30P-rGO-g-C_3N_4 respectively.

3.3.5 Electrocatalytic HER Study

Comparative HER polarization curves of modified GC electrodes along with standard Pt/C (20wt%) are shown in Figure 3.8 (A). Herein, it can be seen that g-C_3N_4 alone is unable to show any significant electrochemical activity in the given potential range. However, the performance of rGO-g-C_3N_4 slightly increases compared to that of g-C_3N_4 alone and touches the current density J = 0.71 mA cm^{-2} at overpotential η = 602 mV owing to the presence 5 wt. % of rGO. rGO alone having an inherent conductive property exhibits a better polarization curve than g-C_3N_4 and rGO-g-C_3N_4 touching current density of 4.46 mA cm^{-2} at the same overpotential value. However, in the case of 30 wt.% phosphorous added ternary

composite we prepared i.e.,30P-rGO-g-C_3N_4 excels among all previous values and exhibits onset potential of -146mV (current density J = 13.38 mA cm^{-2} at overpotential η = 602 mV). This metal-free triad 30P-rGO-g-C_3N_4 requires a 575 mV overpotential value to reach the benchmark current density of 10.00 mA cm^{-2} which is quite good for any earth-abundant element based electrocatalyst. This significant increase in current density value can be attributed to an optimum wt.% of phosphorous added hydrothermally into the composite. LSV plot of 20% Pt/C is also shown which has the best polarization curve among all.

The presence of red phosphorous leads to enhancement in the catalytic performance of the composite. Optimization of the weight amount of P into the composite was done to study the variation in HER performance and get the best current density (*J*) value for the ternary composite. In Figure 3.8 (B), comparative HER polarization curves of various amounts of red phosphorus loaded P-rGO-g-C_3N_4 composites have been shown. We have varied the weight amount of phosphorous from 10% to up to 40% in the composites and LSV was performed in 0.5M H_2SO_4 at a scan rate of 5 mV sec^{-1}. It has been observed that variation in red P loading in the composite P-rGO-g-C_3N_4 from 10 wt. % to up to 30 wt. % causes a linear increase in the *J*-values from 1.02 →2.04 →13.38 mA cm^{-2} at an overpotential value of 602mV for 10P-rGO-g-C_3N_4, 20P-rGO-g- C_3N_4 and 30P-rGO-g-C_3N_4 respectively.

Thus, the *J*-value increases by ~8.84 times in comparison to rGO-g-C_3N_4 with the incorporation of 30% red P at an overpotential of 602mV. Merely, 577 mV of overpotential is required to achieve the current density of 10 mA cm^{-2} for 30P-rGO-g-C_3N_4, while none other composites could touch this value of current density in the entire range. Afterward, when we increase the red P amount to 40 wt. % (40P-rGO-g-C_3N_4), the current density falls to 4.75 mA cm^{-2}.

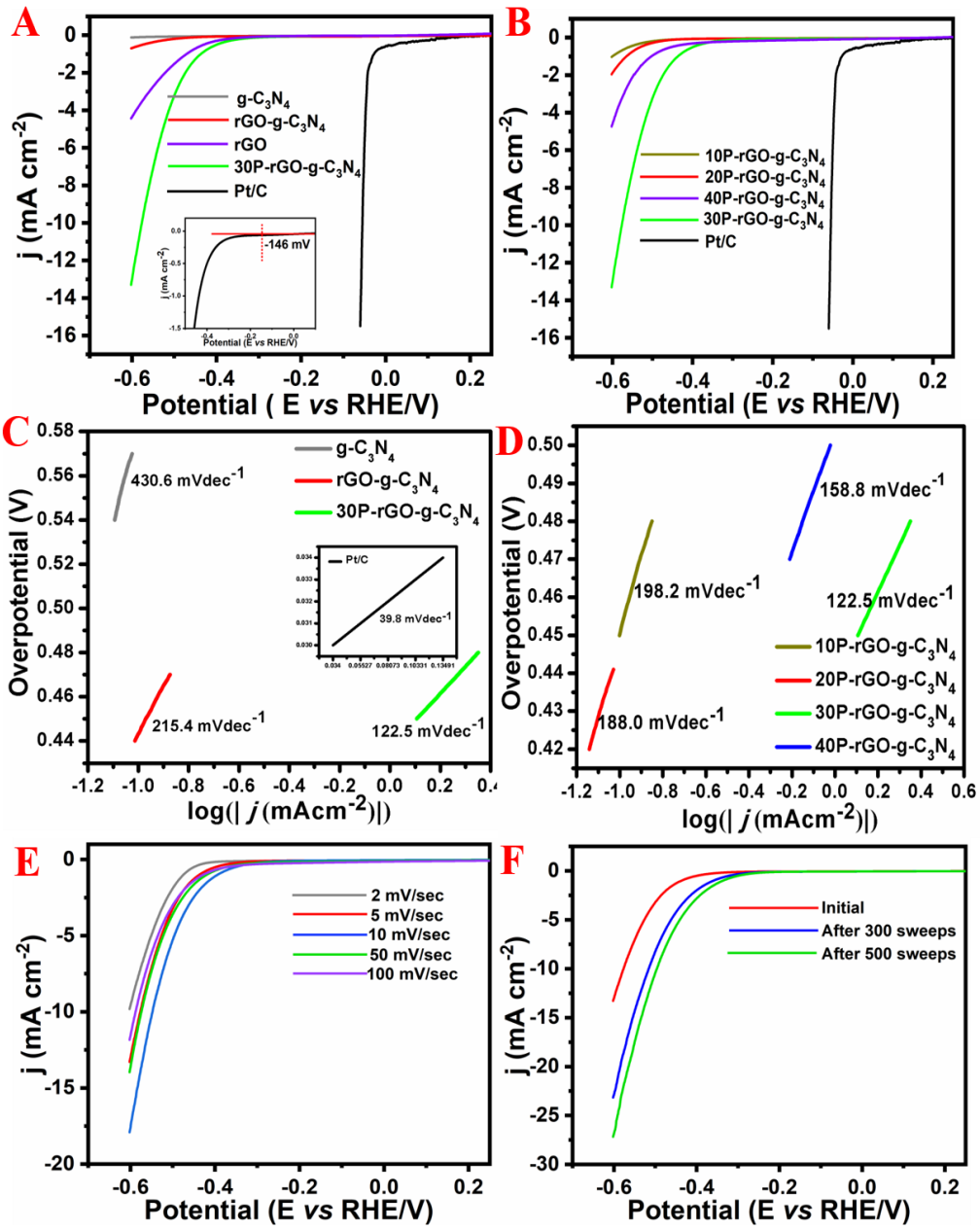

Fig. 3.8 (A) Polarization curves of g-C_3N_4, rGO, rGO-g-C_3N_4, 30P-rGO-g-C_3N_4 and 20% Pt/C in 0.5 M H_2SO_4 at scan rate of 5 mV sec^{-1} (B) Polarization curves of 10/20/30/40P-rGO-g-C_3N_4 along with 20% Pt/C (C) Tafel plots of g-C_3N_4, rGO-g-C_3N_4 and 30P-rGO-g-C_3N_4, in inset 20% Pt/C (D) Tafel plots of 10/20/30/40P-rGO-g-C_3N_4 (E) polarization curves of 30P-rGO-g-C_3N_4 at different can rates and (F) Polarization curves of 30P-rGO-g-C3N4 initially, after 300 sweeps and after 500 sweeps at scan rate of 5 mV sec^{-1}.

Hence, the 30 wt. % of red P is considered the optimum amount in the composite to get the best HER performance. In Figure 3.8 (C) and 3.8 (D), a comparison of the Tafel slope again validates obtained polarization curves of different composites and enhancement in HER performance. It is based on fitting into the Tafel equation (i.e., η = a + b log (*J*); where 'b' is the Tafel slope and '*J'* is the current density; also *see* section 1.4.3.3(c)) and smaller Tafel slope means enhanced HER activity at a small increase of overpotential. [145-151] In Figure 3.8 C we have evaluated slope values of 430.6, 215.4, 122.5 and 39.8 mV dec^{-1} for g-C_3N_4, rGO-g-C_3N_4, 30P-rGO-g-C_3N_4 and 20% Pt/C (in inset) respectively. The Tafel slope value of 121.5mVdec^{-1} for 30P-rGO-g-C_3N_4 is comparatively less to that of rGO-g-C_3N_4 and g-C_3N_4 itself. In case of various red P-rGO-g-C_3N_4 composites (Fig. 3.8 D), we get value of 198.2, 188.0, 122.5 and 158.8 mV dec^{-1} for 10P-rGO-g-C_3N_4, 20P-rGO-g-C_3N_4, 30P-rGO-g-C_3N_4 and 40P-rGO-g-C_3N_4 respectively. These obtained values are in accordance with their HER curves as 30P-rGO-g-C_3N_4 has the lowest Tafel slope among its counterparts. Tafel slope is derived from the Butler-Volmer equation (see for three limiting reactions [62]1. Tafel reaction (combination reaction; 29 mV dec^{-1}), 2. Heyrovsky reaction (Ion + atom reaction; 38mV dec^{-1}) and 3. Volmer reaction (discharge reaction; 120 mV dec^{-1}). In our case, the Tafel slope value of more than 120 mVdec^{-1} indicates the dominance of the Volmer reaction in the desorption of hydrogen from the catalyst surface. In general interpretation, this dominance of Volmer reaction indicates HER preferably proceed via Tafel mechanism. It reveals the improved catalytic behavior and synergistic performance of red P embedded composite.

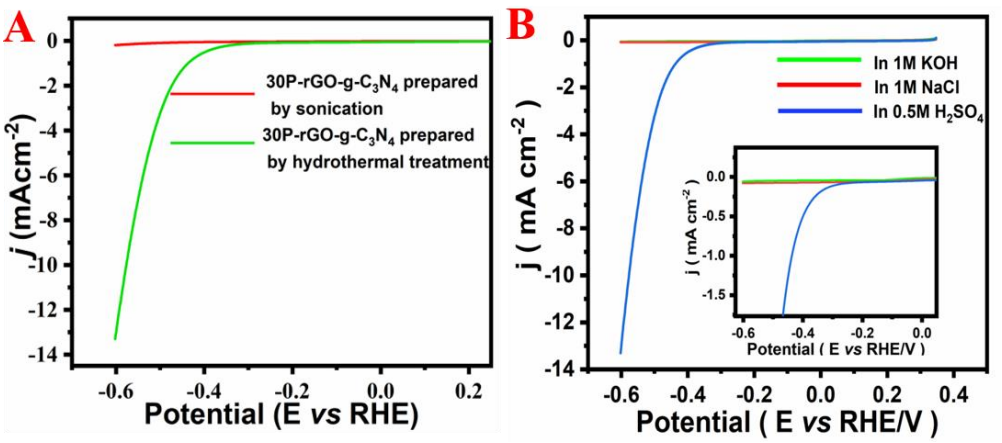

Fig. 3.9 A. Polarization curves of 30P-rGO-g-C_3N_4 prepared by sonication method (physical mixing) and by hydrothermal treatment and B. Polarization curve of 30P-rGO-g-C_3N_4 in neutral, alkali and acidic media. (Scan rate of 5mV/sec in 0.5M H_2SO_4)

The significance of hydrothermal treatment in HER performance was tested by preparing the same composition with 30 wt. % of phosphorous by sonication method and comparing the LSV plot with that of 30P-rGO-g-C_3N_4 prepared hydrothermally. We observed that the composite having 30 wt% of P prepared by sonication method performs badly showing poor activity (current density of merely 0.21 mA cm^{-2}*vs.* 13.38 mA cm^{-2}) at an overpotential of 602 mV (*see* Fig. 3.9 A). Such a robust performance of hydrothermally prepared 30P-rGO-g-C_3N_4 might be attributed to its porosity which leads to greater interaction with electrolyte and excellent intimacies between red P and rGO-g-C_3N_4 composite. We have also performed the LSV measurement of the 30P-rGO-g-C_3N_4 in the neutral (1M NaCl) and alkaline (1M KOH) media and observed negligible catalytic activity (*see* Fig. 3.9 B). Thus, we intended 30P-rGO-g-C_3N_4 composite prepared by hydrothermal treatment for best performance than other ones and checked its various electrochemical behaviors in further experiments. The electrochemical behavior of

30P-rGO-g-C_3N_4 has been further investigated by its HER performance at various scan rates and multiple cycles of CVs (300 and 500 sweeps) to check the viability of 30P-rGO-g-C_3N_4.

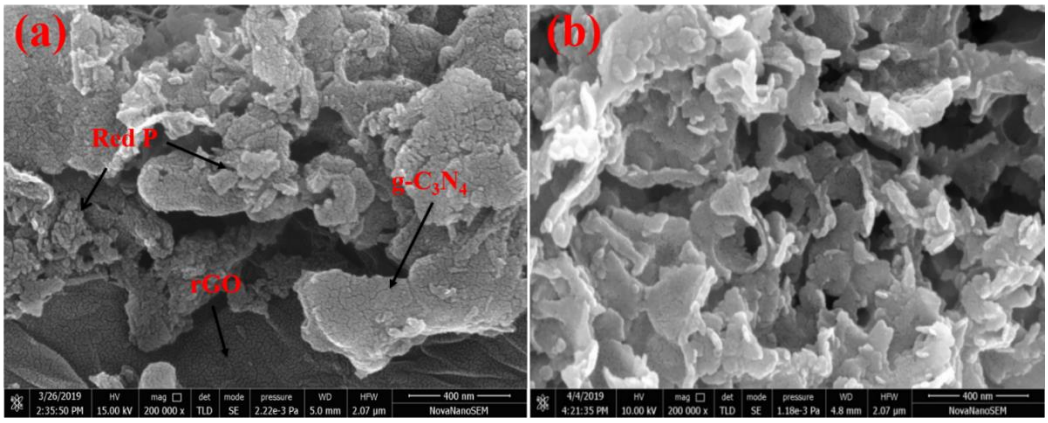

Fig. 3.10 FESEM image of 30P-rGO-g-C_3N_4 before (A) and after (B) performing CVs (300 and 500 sweeps).

Figure 3.8 (E) has LSV curves of 30P-rGO-g-C_3N_4 at various scan rates (*viz.* 2, 5, 10, 50 and 100 mV sec^{-1}), we observe some variation in the amount of current (9.8 mA cm^{-2} for 2 mV sec^{-1} to 11.92 mA cm^{-2} for 100 mV sec^{-1}). The electrochemical stability of 30P-rGO-g-C_3N_4 was further approved by the LSV curves (see Fig. 3.8 (F)) after performing multiple CVs (300 and 500 sweeps). Herein, we also observed that the cathodic current shifts to lower potential due to an increase in porosity of material on repeated cycles of CV resulting in an increase in electrochemical surface area for H^+ ion adsorption. A difference in the porosity can be seen before and after these dynamic applied potentials (*cf.* Fig. 3.10 (a) and 3.10 (b)).

The enhanced hydrogen evolution performance of the 30P-rGO-g-C_3N_4 catalyst might attribute to the synergic effort of all three components present in the

ternary composite. An optimum amount of red P is supposed to provide the best available surface area and active sites, while rGO facilitates faster electron transfer owing to its superior electrical conductivity. The nitrogen of g-C_3N_4 and phosphorous act as active sites and harbour hydrogen ions. Hydrothermal treatment not only degrades the red P size and mangles the sheet structure, but also ensures the creation of more active sites, reduction of GO and greater coordination among constituents for catalytic performance. Therefore, the proper tuning of composition and enhancement in porosity creates greater exposure of active sites and interaction with electrolytes. However, an increase in the phosphorous amount beyond 30 % leads to the reduction in specific surface area of composite (43.778 m^2g^{-1} for 40P-rGO-g-C_3N_4), poor interaction with electrolyte, less availability and density of active sites for H^+ reduction, hence reduction in overall catalytic activity.

Measurement of the electrochemical active surface area (ECASA) is another important parameter to gauge the electrocatalytic performance of a catalyst. Since ECASA is evaluated using double-layer capacitance (C_{dl}) and specific capacitance (Csp), we performed CVs of g-C_3N_4, rGO-g-C_3N_4 and 30P-rGO-g-C_3N_4 under varying scan rates (20 to 200 mV sec^{-1}) in the dynamic potentials range from 0.3 to 0.5 mV. Figure 3.11 (A) has a comparative voltammogram (at scan rate of 100mV sec^{-1}) of g-C_3N_4, rGO-g-C_3N_4 and 30P-rGO-g-C_3N_4 with maximum integrated area for the ternary composite and Figure 3.11 (B) depicts CVs of 30P-rGO-g-C_3N_4 under varying scan rates. The plot of current density difference ($\Delta J = Ja\text{-}Jc$) *vs.* scan rate (Fig. 3.11 (C)) was plotted. All consecutive voltammograms proceed with the non-faradic redox phenomenon and the area under the redox curve increases gradually with an increase in scan rate. Double-layer capacitance was calculated as half of the linear slope which is 94µF cm^{-2}, 487 µF $cm^{-2}$and 590 µF cm^{-2} of g-C_3N_4,

rGO-g-C_3N_4 and 30P-rGO-g-C_3N_4 respectively. It reveals that composite possesses a large number of active surface area and more active sites for H_2 production. Specific capacitance was calculated using equation (Eq. 3.3)

$$C_s = \frac{\int I\, dv}{\Delta V \times k \times m} \quad \text{.....(Eq. 3.3)}$$

Where, the numerator presents integrated area under current-voltage (I-V) curve, 'ΔV' is chosen potential window, 'k' is scan rate in volt/sec and 'm' is mass loading of electrode material.

Now, the electrochemically active surface area was calculated by dividing double-layer capacitance with average specific capacitance, hence ECASA was calculated as 12.26 cm^2g^{-1}, 12.66 cm^2g^{-1} and 14.25 $cm^2g^{-1}$for g-C_3N_4, rGO-g-C_3N_4 and 30P-rGO-g-C_3N_4 respectively.

Current stability at a particular overpotential for a longer time interval is another important criterion to gauge the performance of the catalyst. In order to test the current stability of the 30P-rGO-g-C_3N_4 catalyst, the continuous HER was performed by the Amperometry process under applied static over potential (-670 mV *vs.* Ag/AgCl) for 2 h (7200 seconds) (Fig. 3.11 (D)). A complete setup is shown in Appendix Fig. A.4. It is exemplified that except in the first 200 seconds a constant current stability 72 mA cm^{-2} for a long duration is achieved. However, it shifts to a higher value (increase in *J* value by 5.38% at end of 7200 sec) due to an increase in porosity of the catalyst. This type of increase is also validated in the shift of the LSV curve of the catalyst to lower potential value as explained already in the above case. It is further noted that the surface of the catalyst becomes more odd and porous owing to continuous H_2 formation and release.

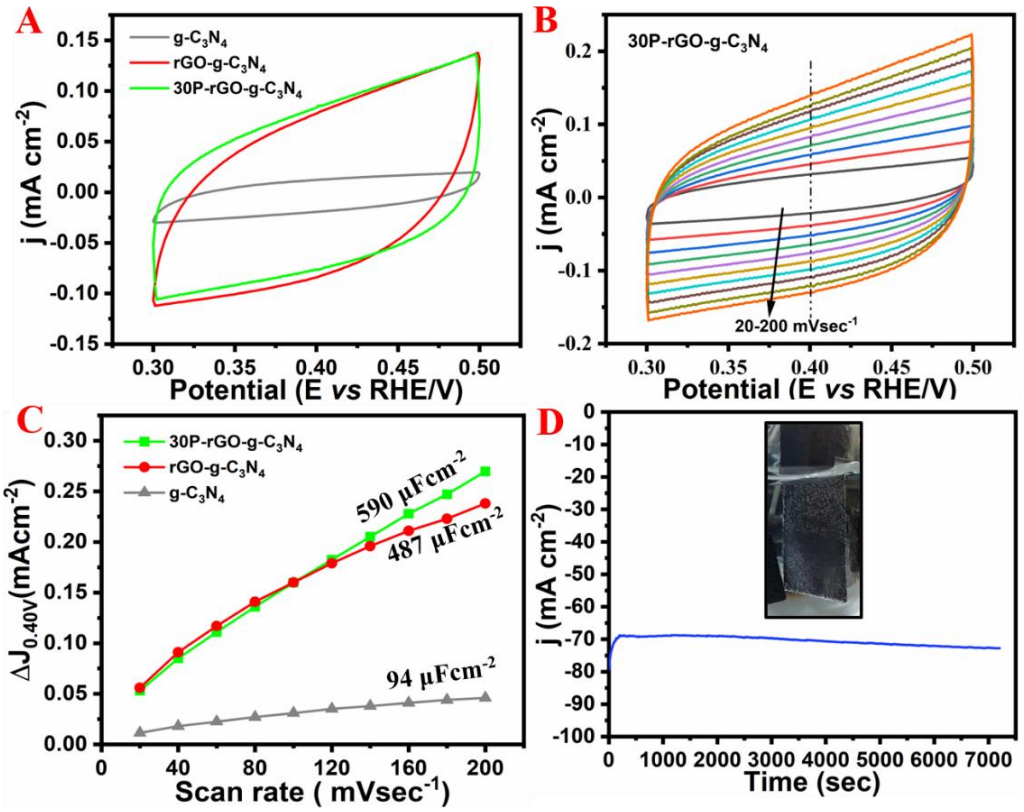

Fig. 3.11 A. Comparative cyclic voltammetry of g-C_3N_4, rGO-g-C_3N_4 and 30P-rGO-g-C_3N_4 at scan rate of 100 mV sec^{-1}; B. CVs of 30P-rGO-g-C_3N_4 at various scan rates; C. electrochemical double-layer capacitance (Cdl) of g-C_3N_4, rGO-g-C_3N_4 and 30P-rGO-g-C_3N_4 and D. Stability test of 30P-rGO-g-C_3N_4 modified Toray paper electrode at a static overpotential of -670mV vs. Ag/AgCl for 2 h (7200 s) in 0.5 M H_2SO_4. The inset Figure shows the generation of H_2 bubbles stationed over the modified Toray paper electrode.

Though the g-C_3N_4 and graphene-based binary catalyst have been reported earlier, but its preparation process involves pre-treatment of g-C_3N_4 either through the complicated steps or usage of a large volume of solvents specially to soften the graphitic carbon nitride or to make it more porous. [122,123] For instance, red P

used in earlier cases possesses crystallization treatment at higher temperature and g-C_3N_4 was vigorously stirred in a concentrated acidic medium for a longer duration to make it porous. [140] These techniques make the catalyst costlier and generate harmful environmental wastes. But our case of study is free from these stimulating conditions and provides more avenues to make use of earth-abundant elements for electrocatalytic hydrogen generations.

3.4 Concluding Remarks

In summary, a triad of red P, rGO and g-C_3N_4 has been prepared successfully by a very simple one-step hydrothermal process. All constituents used are cheap, made up of earth-abundant elements, free from metals and in unmodified form. We have varied the amount of red P in the ternary P-rGO-g-C_3N_4 and observed that an optimum amount of 30 wt. % P is the best to get the maximum HER performance for the composite. The hydrothermal synthesis process enhances the catalytic performance of the composite by an increase in surface area, reduction of GO into rGO, creation of more defects and active sites for H^+ adsorption. The nitrogen of g-C_3N_4 and phosphorous act as active sites to the surface-bound H^+ ions and incorporation of rGO provides a less resistive path for electron transfer through layers. That is why, the ternary 30P-rGO-g-C_3N_4 composite is able to exhibit ~18.84 times higher current density than binary rGO-g-C_3N_4 composite with an onset potential of -146 mV and Tafel slope of 122.5 mV per decade. Our work will open more avenues for the development of metal-free, low-cost, earth-abundant element-based electrocatalyst in other diversified fields.